Nanoscale

An Electrochemical Biosensor Exploiting Binding-Induced Changes In Electron Transfer Of Electrode-Attached DNA Origami To Detect Hundred Nanometer-Scale Targets

Journal:	*Nanoscale*
Manuscript ID	NR-COM-02-2020-000952.R1
Article Type:	Communication
Date Submitted by the Author:	19-May-2020

Complete List of Authors:	Arroyo-Currás, Netzahualcóyotl; Johns Hopkins School of Medicine, Department of Pharmacology and Molecular Sciences Sadeia, Muaz; St John's University, Chemistry Ng, Alex; St John's University, Chemistry Fyodorova, Yekaterina; St John's University, Chemistry Williams, Natalie; St John's University, Chemistry Afif, Tammy; St John's University, Chemistry Huang, Chao-Min; Ohio State University Department of Mechanical and Aerospace Engineering, Mechanical and Aerospace Engineering Ogden, Nathan; UCSB, Chemistry and Biochemistry Andresen Eguiluz, Roberto; UCSB, Chemistry and Biochemistry Su, Haijun; Ohio State University Department of Mechanical and Aerospace Engineering Castro, Carlos; Ohio State University Department of Mechanical and Aerospace Engineering, Mechanical and Aerospace Engineering Plaxco, Kevin; UCSB, Chemistry and Biochemistry Lukeman, Philip; St John's University, Chemistry

COMMUNICATION

An Electrochemical Biosensor Exploiting Binding-Induced Changes In Electron Transfer Of Electrode-Attached DNA Origami To Detect Hundred Nanometer-Scale Targets

Received 00th January 20xx,
Accepted 00th January 20xx

DOI: 10.1039/x0xx00000x

Netzahualcóyotl Arroyo-Currás,[b] Muaz Sadeia,[a] Alexander K. Ng,[a] Yekaterina Fyodorova,[a] Natalie Williams,[a] Tammy Afif,[a] Chao-Min Huang,[d] Nathan Ogden,[c] Roberto C. Andresen Eguiluz,[c] Hai-Jun Su,[d] Carlos E. Castro,[d] Kevin W. Plaxco[c] and Philip S. Lukeman[*a]

The specific detection in clinical samples of analytes with dimensions in the tens to hundreds of nanometers, such as viruses and large proteins, would improve disease diagnosis. Detection of these "mesoscale" analytes (as opposed to their nanoscale components), however, is challenging as it requires the simultaneous binding of multiple recognition sites often spaced over tens of nanometers. In response, we have adapted DNA origami, with its unparalleled customizability to precisely display multiple target-binding sites over the relevant length scale, to an electrochemical biosensor platform. Our proof-of-concept employs triangular origami covalently attached to a gold electrode and functionalized with redox reporters. Electrochemical interrogation of this platform successfully monitors mesoscale, target-binding-induced changes in electron transfer in a manner consistent with coarse-grained molecular dynamics simulations. Our approach enables the specific detection of analytes displaying recognition sites that are separated by ~ 40 nm, a spacing significantly greater than that achieved in similar sensor architectures employing either antibodies or aptamers.

DNA origami[1] – the Watson-Crick controlled folding of a long DNA scaffold strand using hundreds of short, rationally designed oligonucleotide "staples" – enables the construction of nanoscale objects, including devices capable of computation, molecular recognition, and response to specific molecular stimuli[2]. Modification of origami with recognition elements for specific small molecules, nucleic acids or proteins enables their use in biosensing[3] often using binding-induced changes to produce a fluorescent or plasmonic output[4, 5]. Optical approaches fail, however, at analyte detection in biological fluids, an ability necessary for the direct sensing of analytes in clinical settings.

In contrast to optical approaches, electrochemical sensors that rely on structure-switching signal transduction successfully achieve molecular detection in biological fluids[6]. In this the binding-induced conformational change of an electrode-bound redox-reporter-modified receptor produces a measurable change in electrochemical output[7]. Given the specificity of this signal transduction mechanism, such sensors have proven particularly well suited for performing prolonged measurements in whole blood[8, 9].

Origami is capable of supporting binding-induced electrochemical outputs but this has yet to be demonstrated. Instead, non-electrophoretic experiments involving the exposure of origami to electric fields have been limited to origami pore conductivity measurements[10-12] control of origami fluorescent switches[13], electromechanical actuation of origami levers[14] and fluorescent readout of voltage-controlled origami movement[15]. Recently, electrochemical analysis of surface-bound origami has been used to detect ss-miRNA[16] and to probe spatial determinants of redox-active enzyme activity [17]. However, none of these approaches appear to be generalizable in a manner that could exploit binding-induced changes in electrochemical detection as a means of signal transduction. This mode of detection could enable the measurement of clinically relevant, mesoscale analytes such as large proteins and whole viruses (rather than their subcomponents), a feat that is undemonstrated with current DNA-based platforms.

Motivated by these arguments, we report here the first electrochemical biosensors employing full-size (~5 MDa) origami, which we use to sense the binding of mesoscale analytes with multiple target-binding sites separated by ~40 nm.

[a] *Department of Chemistry, St. John's University, Queens, NY 11439, USA E-mail: lukemanp@stjohns.edu*
[b] *Department of Pharmacology and Molecular Sciences, Johns Hopkins University School of Medicine, Baltimore, MD 21205, USA.*
[c] *Department of Chemistry and Biochemistry, Center for Bioengineering and Department of Chemical Engineering, University of California Santa Barbara, Santa Barbara, CA 93106, USA*
[d] *Department of Mechanical and Aerospace Engineering/Biophysics Graduate Program, The Ohio State University, Columbus, Ohio 43210, USA*

†Electronic Supplementary Information (ESI) available: All experimental details, characterization of Origami and binding, further electrochemical experiments, MATLAB code for real-time electrochemical analysis, sequences, and more detailed simulations. See DOI: 10.1039/x0xx00000x.

This paper is dedicated to the memory of Arnold Lukeman – chemist, teacher and father.

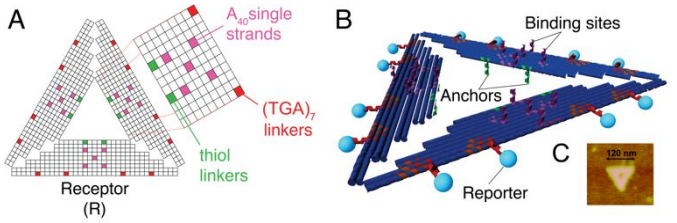

Fig. 1. The DNA origami "Receptor", is a 2 nm thick single-layer triangle 120 nm on each side[1,17] **A**) In this scheme, squares represent positions on each triangle where we functionalized the staples' termini as follows: Red = TGA_7 linkers, 4 per outer edge, pointing "outwards" in the plane of the triangle - these linkers were bound to complementary, redox-reporter displaying strands. The redox reporters are methylene blue molecules appended to the 5' end of TCA_7 strands ("MB-strands"). The MB-strands include a 3' single-stranded 7-nt "toehold, that enables their displacement when complementary "anti-strands" are added (Fig S19, Fig. 2). Green = anchor thiols, two per inner edge on the "bottom" of the triangle with $HS-(CH_2)_6-PO_4-(CH_2)_6-$ linkers connected to their 5' ends. Magenta = Target binding sites: 3'-A_{40} single strands, five per side, ends projecting out of the "top" of the triangle. The inset displays a zoomed-in area of the triangle. **B**) Three-dimensional representation of the receptor; the light blue balls are Methylene Blue reporters. **C**) Representative AFM image of the Receptor (more in Fig. SB).

To synthesize the "Receptor" component of our sensor, we modified a literature triangle design[1, 18] with twelve signal-generating, DNA duplexes functionalized with Methylene Blue that project these redox reporters laterally from its outer edges, six thiol-modified "surface anchors" projecting down from the inner edge's "bottom" face, and fifteen target-binding A_{40} strands projecting up from the centers of its "top" face (Fig. 1A, B). We covalently attached these receptors to a 1,6-hexanedithiol self-assembled monolayer (SAM) formed on the surface of smooth gold electrodes. We employed the SAM for the purposes of 1) passivating the gold surface, preventing non-desired electrochemical reactions and 2) to provide strong anchoring points for the receptors. After testing various surface preparations (Fig. S1) and SAM-forming reagents (Figs. S2, S3) we ultimately chose 1,6-hexanedithiol on electrochemically cleaned, e-beam deposited gold because it forms reproducible, smooth, densely packed and highly oriented SAMs[19] (Fig. S4) with large receptor-originated faradic currents (Figs. S2, S3).

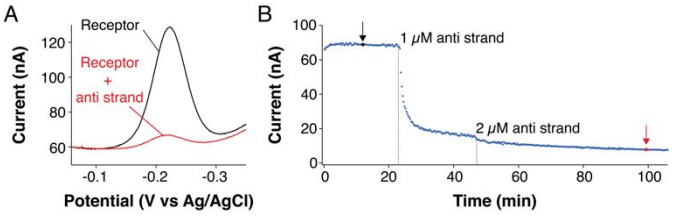

Fig. 2. Square-wave voltammetry measures the reduction of redox reporter-modified, surface bound origami receptors. The faradaic current originates from the reduction of MB-strands on receptor edges, as opposed to free MB-strands in solution. **A)** Voltammograms corresponding to measurement we performed on reporter-containing origami (black) versus origami treated with an anti-strand to displace MB-strands (red). **B)** A time-course experiment in which we interrogated the system every 15 s for 80 min – we added anti-strand at 20 and 45 min. The anti-strand effectively displaced most of the MB-strands from the receptor, causing a steep drop in voltammetric peak currents. The arrows indicate peak currents corresponding to the voltammograms in panel A.

We interrogated the origami-based sensor using square-wave voltammetry. As an aid in maximizing sensor response, we determined the dependence of the reduction current on square-wave frequency[20-22] (Fig. S5); a frequency of 60 Hz produces voltammograms with the largest signal-to-noise ratio, giving 20-80 nA peak currents for a 3.15 mm^2 electrode (Fig. 2A)

To show that these currents originate specifically from the electrochemical reduction of the origami's methylene blue-modified strands ("MB-strands"), we equipped these with 7-base single-stranded "toeholds," allowing their displacement (Fig. S19) from the triangle edges via the introduction of fully complementary "anti-strands"[23]. When challenged with 1 μM of the anti-strand, peak current fell by 78% (Fig. 2B); when pushed to 2 μM the current fell by 90%, indicating displacement of the MB-strands from the surface-bound origami (Figs. S6, S7).

The origami-based sensor selectively responds to its polyvalent target. To demonstrate this we designed three target origami triangles as follows (Fig. 3A-C): 1) a non-binding target, K_{NC}, containing five non-complementary A_{40} DNA strands on each of its three sides; 2) a single-sided target, K1, decorated with five T_{40} strands on one of its three sides; and 3) the polyvalent triple-sided, rigid target, K3, decorated with five T_{40} strands on each of its three sides and rigidified by the addition of staple linkers between its internal trapezoidal edges. We challenged our sensor with each of these targets while continuously monitoring their square-wave voltammograms every 15 s (Fig. 3D).

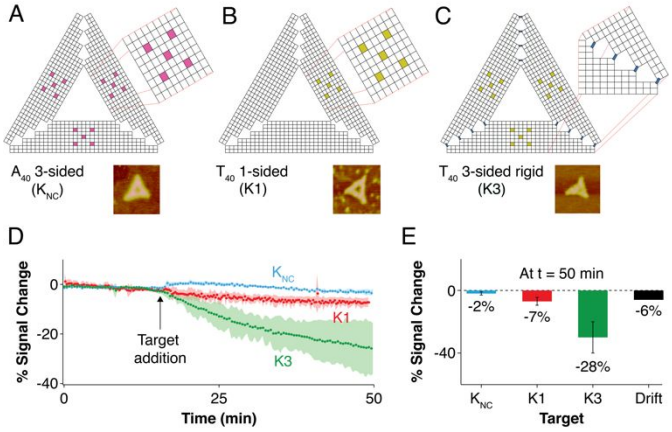

Fig. 3. The binding of polyvalent target triangles produces an easily measurable change in electron transfer. To test the ability of our platform to electrochemically detect large analytes we designed three target origami triangles as follows: A) K_{NC} presents five 3' A_{40} single strands per side projecting out of the "top" of the triangle (magenta). These are not complementary to the target-binding sites on the receptor; K_{NC} serves as a non-binding control; B) K1 presents five complementary 5' T_{40} strands projecting out of the top of a single side of the triangle (dark yellow); C) K3 presents five complementary 5' T_{40} strands projecting out of the top of each of its three sides (dark yellow). K3 contains T_3, T_2, T_1 and zero-base staple linkers (blue) bringing the trapezoidal edges into greater proximity[1] – each blue attachment point of these linkers is held with two 11-base flanking sequences that are complementary to the scaffold and thus rigidify the trapezoidal edges. Inset displays a zoomed-in area of the triangle edge, representative AFM images of K_{NC}, K1 and K3 are shown (More in Fig. SB). D) Time-course studies in which we challenged DNA origami-functionalized electrodes with targets K_{NC}, K1, and K3. The shaded areas represent the standard deviation between three independently fabricated electrodes. E) Plot of relative signal change 50 min after the addition of targets. The bar corresponding to drift was calculated based on the slopes of K_{NC}, K1 and K3 time-course experiments between t = 0 and 20 min (prior to the addition of targets).

Challenging with target K3 produces a monotonic decrease in signaling current equilibrating at -28% after 50 min, serving as proof-of-concept to demonstrate electrochemical sensing of polyvalent targets across distances of ~40 nm. That is, we posit that the observed decrease is driven by the polyvalent binding of K3, which, by having three sets of target-binding sites and extra rigidity via linker staples on its internal trapezoidal edges, binds to R (Fig. SA), causing it to undergo a structural change. This change, in turn, results in the redox reporters on R undergoing fewer interactions with the surface, thus decreasing the observed current (Fig. S5). Challenging the sensor with K1, in contrast, produces only a small decrease in peak current, equilibrating after ~50 min at -7%. This decrease is not statistically different from the intrinsic drift (-6%) of the system. We posit that this occurs because, although K1 does bind to R (Fig. SA), the binding does not deform R in a manner that significantly changes electron transfer. This might be expected as K1 displays complementary binding sites on only one side of the triangle, suggesting that it will bind to only a single side of R. Finally, as expected the addition of the non-complementary, non-binding (Fig. SA) control KNC to the sensor produced only a small (~2%), instantaneous increase in peak current that returned to baseline levels after 30 min (Fig. 3). Gel-shift analysis of all three target-receptor complexes when free in bulk solution confirms that strand displacement does not occur upon target binding (Fig. SA), and AFM analyses of all triangles indicates they fold to the expected dimensions (Fig. SB).

The specific decrease in signaling current generated by K3 is caused by a reduction in the structural flexibility of R. We demonstrate this by employing a previously described computational workflow,[24] featuring the OxDNA molecular dynamics package,[25-27] to simulate fluctuations in the spatial positioning of redox reporters (Fig. 4) in the systems R, R+K1 and R+K3. These simulations indicate that, upon binding K3, R undergoes a change in structural rigidity, which dampens the ability of the reporters to approach the electrode closely enough to transfer electrons.

The results presented here demonstrate the engineering of origami-based electrochemical biosensors for the detection of mesoscale targets, a target length scale not accessible to any other rationally customizable sensing platform reported to date that can perform in complex biological matrices. The closest analogous self-assembled nanostructure that is utilized in electrochemical biosensing are 10 nm-scale DNA tetrahedra. These tetrahedra are mostly exploited as rigidifying spacers modified with a single recognition element (e.g., an aptamer); the tetrahedron itself is not directly involved in binding-induced signal transduction[3]. Although tetrahedra have been used to compare through-space and through-duplex electron charge transfer[28],and to monitor low nanometer-scale binding events by displacing a DNA strand using a single ferrocene-labeled terahedron[29] by virtue of their size and simplicity they cannot perform recognition over length scales accessible to origami, nor radically improve signaling capability compared to their appended recognition element.

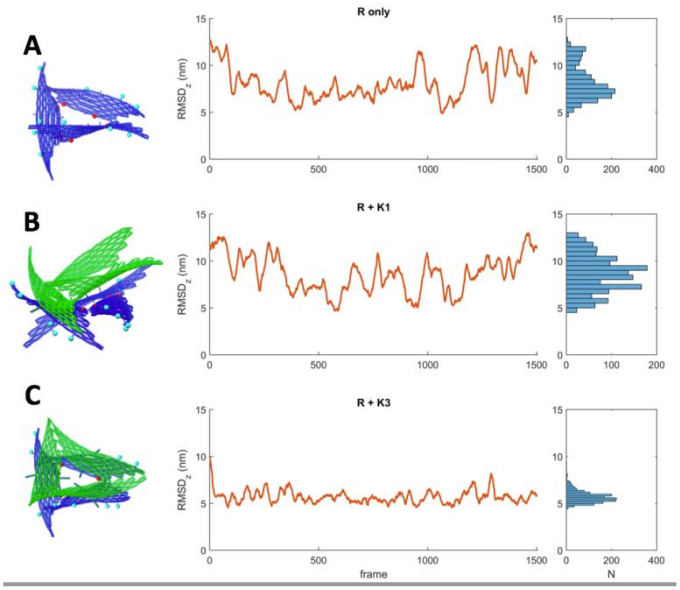

Fig. 4: OxDNA simulations of the Receptor show a decrease in redox reporter positional fluctuations upon binding K3; there is no significant fluctuation decrease upon binding of K1. The root mean square deviation (RMSD) in the z-direction, which is normal to the reference plane of the triangle (i.e. plane containing the 6 points where the R structure is anchored) was calculated with respect to the average configuration shown at left (averaged over the 1500 frames) for all three cases: (A) R alone, (B) R+K1, and (C) R+K3. The traces show the RMSD values averaged over the 12 redox reporter sites (blue circles at left). The data were smoothed using a 20-point moving average, and in these traces one frame corresponds to approximately 1 μs. We observed large fluctuations in the position of the redox reporters for both the R and R+K1 constructs, and these fluctuations were dampened for the R+K3, as clearly illustrated by the distributions of RMSD (right), indicating binding of K3 makes the complex significantly stiffer, which likely reduces the number of interactions between the redox labels and the electrode surface.

DNA origami-based electrochemical sensing offers the ideal approach to the measurement of clinically relevant mesoscale analytes. This is because 1) origami offers molecular surfaces that can accommodate mesoscale arrays of target binding sites and 2) origami can be rationally designed to produce target binding-induced signaling across larger distances than conventional DNA-based sensors. For example, single-layer origami could achieve the specific detection of viruses by displaying arrays of viral-capsid-binding aptamers[30] with an inter-aptamer resolution of ~2 nm, displaying tens of aptamers across mesoscale distances. If greater spatial resolution in the placement of target binding sites, anchors or redox reporters is required, multilayer origami can be designed to display these functional groups with sub-ångström precision[31].

Beyond offering unprecedented structural customizability for target recognition, origami-based sensors could also overcome inherent limitations of electrochemical biosensors that rely on single or double stranded nucleic acids for detection. For example, origami can be selectively modified with hundreds of fluorescent[32] or redox reporters, as opposed to just a few reporters in single-stranded, double-stranded or DNA tetrahedra. This would improve the detection of single analytes by increasing the signal-to-noise ratio of electrochemical signaling. Moreover, redox reporters and target binding sites are locatable on separate strands in the origami; thus their position and flexibility can be tuned at will.

This should enable the signal gain of an origami-based sensor to be maximized by design, instead of being limited by the length or flexibility of a single or double strand, as is the case of conventional DNA sensors.

Other powerful features of the proposed electrochemical origami-based sensing approach are the possibility of improving its resistance to degradation in harsh environments by using crosslinking[33, 34] or other strategies[35], and the fact that mesoscale target detection has historically been hard to achieve but is readily supported by origami[18]. Moreover, the simplicity of placing origami on lithographically patterned surfaces[36] could enable the multiplexed detection of many of these large biological targets on electronic sensor arrays, with the potential ability to create biomolecular profiles of disease states, a feat not achievable with current technologies. And because electrochemistry-based sensing readily supports measurements in biological fluids[9, 37], origami-based electrochemical detection could support these measurements in whole blood *in vitro* and *in vivo*. Overall, the approach described here offers an unprecedented opportunity to realize truly customized, direct detection of specific, clinically-relevant mesoscale targets.

Author Contributions

This project was conceived by PSL with formative and substantive conceptual input from NA and KWP. NA designed, optimized and ran electrochemical experiments with PSL. MS, AKN, YF, NW, TA and PSL designed, synthesized and characterized the origami and conducted AFM analyses. CMH designed and ran simulations under the supervision of HJS and CEC. NA and RCAE synthesized and analyzed the gold substrates. NA, CEC, KWP and PSL wrote the paper.

Conflicts of interest

The Authors declare no conflicts of interest.

Acknowledgements

PSL is grateful for support from Army Research Office (Awards W911NF-16-1-0178 and W911NF-19-1-0326). PSL thanks Paul Rothemund and Gabriel Ortega for insightful discussions. PSL also thanks LukemanLab members for their hard work; particularly Christopher Chen and Ekaterina Selivanovitch for preliminary study of the triangle.

Notes and references

1. P. W. K. Rothemund, *Nature*, 2006, **440**, 297.
2. F. Hong, F. Zhang, Y. Liu and H. Yan, *Chem. Rev.*, 2017, **117**, 12584-12640.
3. N. Xie, S. Liu, X. Yang, X. He, J. Huang and K. Wang, *Analyst*, 2017, **142**, 3322-3332.
4. M. Pilo-Pais, G. P. Acuna, P. Tinnefeld and T. Liedl, *MRS Bull.*, 2017, **42**, 936-942.
5. P. Wang, T. A. Meyer, V. Pan, P. K. Dutta and Y. Ke, *Chem*, 2017, **2**, 359-382.
6. K. W. Plaxco and H. T. Soh, *Trends Biotechnol.*, 2011, **29**, 1-5.
7. L. R. Schoukroun-Barnes, F. C. Macazo, B. Gutierrez, J. Lottermoser, J. Liu and R. J. White, *Annu. Rev. Anal. Chem.*, 2016, **9**, 163-181.
8. B. Feldman, R. Brazg, S. Schwartz and R. Weinstein, *Diabetes technology & therapeutics*, 2003, **5**, 769-779.
9. N. Arroyo-Currás, J. Somerson, P. A. Vieira, K. L. Ploense, T. E. Kippin and K. W. Plaxco, *Proc Natl Acad Sci U S A*, 2017, **114**, 645-650.
10. B. R. Aryal, T. R. Westover, D. R. Ranasinghe, D. G. Calvopiña, B. Uprety, J. N. Harb, R. C. Davis and A. T. Woolley, *Langmuir*, 2018, **34**, 15069-15077.
11. S. Hernández-Ainsa, K. Misiunas, V. V. Thacker, E. A. Hemmig and U. F. Keyser, *Nano Lett.*, 2014, **14**, 1270-1274.
12. J. R. Burns, A. Seifert, N. Fertig and S. Howorka, *Nat. Nanotechnol* .2016, **11**, 152.
13. X. Wang, C. Li, D. Niu, R. Sha, N. C. Seeman and J. W. Canary, *Nano Lett.*, 2018, **18**, 2112-2115.
14. F. Kroener, A. Heerwig, W. Kaiser, M. Mertig and U. Rant, *J. Am. Chem. Soc.*, 2017, **139**, 16510-16513.
15. E. A. Hemmig, C. Fitzgerald, C. Maffeo, L. Hecker, S. E. Ochmann, A. Aksimentiev, P. Tinnefeld and U. F. Keyser, *Nano Lett.*, 2018, **18**, 1962-1971.
16. S. Han, W. Liu, S. Yang and R. Wang, *ACS Omega*, 2019, **4**, 11025-11031.
17. Z. Ge, J. Fu, M. Liu, S. Jiang, A. Andreoni, X. Zuo, Y. Liu, H. Yan and C. Fan, *ACS Appl. Mater. Interfaces*, 2018, **11**, 13881-13887.
18. N. Stephanopoulos, M. Liu, G. J. Tong, Z. Li, Y. Liu, H. Yan and M. B. Francis, *Nano Lett.*, 2010, **10**, 2714-2720.
19. D. Qu, B.-C. Kim, C.-W. J. Lee, M. Ito, H. Noguchi and K. Uosaki, *The Journal of Physical Chemistry C*, 2009, **114**, 497-505.
20. Š. Komorsky-Lovrić and M. Lovrić, *Electrochim. Acta*, 1995, **40**, 1781-1784.
21. V. Mirčeski and M. Lovrić, *Electroanalysis*, 1997, **9**, 1283-1287.
22. M. Lovrić and Š. Komorsky-Lovric, *J. Electroanal. Chem.*, 1988, **248**, 239-253.
23. D. Y. Zhang and G. Seelig, *Nature chemistry*, 2011, **3**, 103.
24. C.-M. Huang, A. Kucinic, J. V. Le, C. E. Castro and H.-J. Su, *Nanoscale*, 2019, **11**, 1647-1660.
25. J. S. Schreck, F. Romano, M. H. Zimmer, A. A. Louis and J. P. Doye, *ACS nano*, 2016, **10**, 4236-4247.
26. B. E. Snodin, F. Romano, L. Rovigatti, T. E. Ouldridge, A. A. Louis and J. P. Doye, *ACS nano*, 2016, **10**, 1724-1737.
27. R. Sharma, J. S. Schreck, F. Romano, A. A. Louis and J. P. Doye, *ACS nano*, 2017, **11**, 12426-12435.
28. N. Lu, H. Pei, Z. Ge, C. R. Simmons, H. Yan and C. Fan, *J. Am. Chem. Soc.*, 2012, **134**, 13148-13151.
29. A. Abi, M. Lin, H. Pei, C. Fan, E. E. Ferapontova and X. Zuo, *ACS Applied Materials & Interfaces*, 2014, **6**, 8928-8931.
30. P. S. Kwon, S. Ren, S.-J. Kwon, M. E. Kizer, L. Kuo, M. Xie, D. Zhu, F. Zhou, F. Zhang, D. Kim, K. Fraser, L. D. Kramer, N. C. Seeman, J. S. Dordick, R. J. Linhardt, J. Chao and X. Wang, *Nat Chem.*, 2020, **12**, 26-35..
31. J. J. Funke and H. Dietz, *Nat Nanotechnol.*, 2016, **11**, 47.
32. D. Selnihhin, S. M. Sparvath, S. Preus, V. Birkedal and E. S. Andersen, *Acs Nano*, 2018, **12**, 5699-5708.
33. V. Cassinelli, B. Oberleitner, J. Sobotta, P. Nickels, G. Grossi, S. Kempter, T. Frischmuth, T. Liedl and A. Manetto, *Angew. Chem. Int. Ed.*, 2015, **54**, 7795-7798.
34. T. Gerling, M. Kube, B. Kick and H. Dietz, *Sci. Adv.*, 2018, **4**.
35. N. Ponnuswamy, M. M. Bastings, B. Nathwani, J. H. Ryu, L. Y. Chou, M. Vinther, W. A. Li, F. M. Anastassacos, D. J. Mooney and W. M. Shih, *Nat. Commun.*, 2017, **8**, 15654.
36. R. J. Kershner, L. D. Bozano, C. M. Micheel, A. M. Hung, A. R. Fornof, J. N. Cha, C. T. Rettner, M. Bersani, J. Frommer and P. W. Rothemund, *Nat. Nanotechnol.*, 2009, **4**, 557.
37. N. y. Arroyo-Currás, G. Ortega, D. A. Copp, K. L. Ploense, Z. A. Plaxco, T. E. Kippin, J. o. P. Hespanha and K. W. Plaxco, *ACS Pharmacology & Translational Science*, 2018, **1**, 110-118.

Using DNA origami as the recognition element in an electrochemical biosensor enables the selective and direct detection of "mesoscale" virus-sized analytes.